19th Brazilian Congress of Thermal Sciences and Engineering
November 6th–10th, 2022, Bento Gonçalves - RS - Brazil

ENC-2022-0376
ANALYSIS OF 1D HEAT AND MASS TRANSFER MODELS FOR AIR DEHUMIDIFICATION USING SOLID DESICCANTS

Jael Yankson
Maurício de Souza Maciel
Leandro Alcoforado Sphaier
Laboratory of Thermal Sciences (LATERMO), Department of Mechanical Engineering, Universidade Federal Fluminense (PG-MEC/UFF), Rua Passo da Pátria 156, bloco E, sala 206-D, Niterói, RJ 24210-240, Brazil
jaelyankson@id.uff.br, mauriciomaciel@id.uff.br, lasphaier@id.uff.br

Abstract. *The use of solid desiccants has played an important role in air conditioning systems with the purpose of dehumidifying atmospheric air based on its energy efficiency. This paper is aimed at investigating heat and mass transfer in solid desiccants using silica gel. Two types of desiccant dehumidifier models are recalled, one based on a fixed-bed system, and another on desiccant-coated channels. Both formulations are then shown to be analogous by defining an equivalent matrix porosity. Then, dimensionless groups relevant to the considered problem are present, which are shown to fully normalize the problem. Almost finally, the equations are solved using the Finite Volume Method for spatial discretization, the Method of Lines for time-integration solution, using the numerical routines built in the Mathematica system. A mesh verification study is carried out to determine the proper mesh for simulations. At last, in order to illustrate the effect of dimensionless groups simulation results of a few cases are presented.*

Keywords: *Mathematical Model, Physical Adsorption, Desiccant Wheel, Fixed-Bed, Rotary Exchanger*

NOMENCLATURE

$\mathcal{A}_p$	channel flow area
$\mathcal{A}_f$	channel wall area
c	specific heat
C	heat capacity
h	convective transfer coefficient
i_{sor}	heat of sorption
L	channel lenght
m	mass
NTU	number of transfer units
$\mathcal{P}_s$	wetted perimeter
T	temperature
$\mathcal{S}$	specific area
t	time
v	average bulk velocity (parallel to flow direction)
V	volumetric capacity
$\mathcal{V}$	volume
W	concentration in adsorbed phase
x	spatial coordinate
Y	dry basis vapor concentration

Greek Symbols

ε	porosity

ρ density or specific mass
τ_{dw} dwell time

Subscripts and superscripts

$(\ )_a$ dry air
$(\ )_b$ bed
$(\ )_e$ effective property
$(\ )_h$ sensible heat transfer
$(\ )_l$ water in adsorbed phase
$(\ )_m$ mass transfer
$(\ )_p$ desiccant particle (or desiccant wall)
$(\ )_r$ ratio
$(\ )_s$ dry solid phase of desiccant
$(\ )_v$ water vapor
$(\ )^i$ sensible portion
$(\ )^p$ latent portion
$(\ )^*$ dimensionless property

1. INTRODUCTION

Today, the world is facing one of its biggest challenges to control and minimize the effects of climate change mainly due to our unsustainable energy use over the last century. Nowadays, most countries are adapting to different alternatives for sustainable energies with high efficiency and a lower environmental impact. In most tropical countries, dehumidification of air through air conditioning is an essential operation, but also a problem due to its high cost. Jani *et al.* (2016) has shown the high amount of electrical energy typically consumed during this process. Zhao *et al.* (2015), and Wu *et al.* (2018) presented the environmental risk involved in conventional air dehumidification. A recent study conducted by Li *et al.* (2010) mentioned that the consumption of energy with a conventional air conditioning during summer periods could exceed 50% of the total energy consumption. Hence, dehumidifying the incoming air is essential to overcome this situation. One such alternative involves, driving the moist air through a solid desiccant to produce a dry airstream. Solid desiccants comprise compounds that can adsorb the water vapor as a result of the difference in partial vapor pressure between the desiccant surface and the surrounding air (Beery and Ladisch, 2001). Today, there are various solid desiccants commercially available among these are silica gel, activated alumina, activated charcoal, zeolite and etc (Dai *et al.*, 2001).

The use of solid desiccants for cooling applications are mainly found in the form of desiccant cooling cycles, which have been a main subject of study over last decades (DAOU *et al.*, 2006). It has been shown that the reduction of the latent heat load through air dehumidification by adsorption on hygroscopic materials is a viable alternative to traditional forms of cooling cycles. While conventional cooling cycles use working fluids potentially harmful to the environment, desiccant cycles use water. Allied to this, there is also the possibility of using thermal waste from previous processes as energy source for evaporative cooling, which leads to a reduction in the consumption of the so-called"high-grade energies."

The main component in a desiccant cooling cycle is the dehumidifier, which for the majority of applications is found in the form of a desiccant wheel. These are regenerative heat and mass exchangers with a multitude of mini-channels coated with a hygroscopic material (generally silica gel), that operate between a process stream and a regeneration stream. Introductory studies focused on this type of equipment were published in the early 20th century. Rudimentary models hypothesized isothermal mass transfer along the porous channel Hougen and Marshall (1947). Many approaches to the problem have been explored over time. Most investigations involve one-dimensional formulations for both convection and diffusion studies in solid material Chung *et al.* (2009); Shang and Besant (2009); Ge *et al.* (2010). However, more sophisticated models have been under study since the beginning of the 21st century. Sphaier and Worek (2004) proposed a multidimensional study model for both heat exchange and diffusion at the adsorbent surface, which includes both sensible heat wheels (or enthalpy exchangers) and desiccant wheels. Ruivo *et al.* (2007) employed a 2-D model of diffusion and convection, and compared the study to a simplified 1-D model, showing that simplified studies can be employed under certain conditions. In the second half of the last decade, Cheng *et al.* (2016, 2017) have done similar work, comparing sophisticated models presenting multidimensional formulation for diffusion to simplified one-dimensional models. Despite the possibility of simplifying multidimensional models to one-dimensional ones under certain circumstances as seen above, there is little information on the behavior of convective coefficients in multidimensional models, a topic that was the subject of study of Santos and Sphaier (2020). Recently, Jedlikowski *et al.* (2020) performed a one-dimensional study using a partial differential equations model solved by the finite difference method for heat and mass transfer in rotational exchangers operating under high rotor speed conditions. Similarly, Zhehuadu and Lin (2020) also used partial differential equations solved by the finite difference method, but in this work the model used was two-dimensional for the desiccant wheel axial and radial axes, and very low speed conditions set for the rotational heat exchanger.

Although most cooling cycles rely on desiccant wheels, there are cases for which a different type of dehumidifier may be required. For applications involving pressurized air for instance, leakage may become a problem in rotary regenerative

devices, such as desiccant wheels. This may be circumvented by using sealed pressurized vessels filled with desiccant particles, comprising adsorption in a porous fixed bed. A simple model for the dehydration of natural gas in this type of configuration as proposed by Benther and Sphaier (2015), which could be easily adapted for moist air applications. In this sense, the purpose of this work is to analyze two types of formulations used for dehumidification with solid desiccants, namely mini-channels coated with hygroscopic materials (i.e. desiccant wheels) and porous fixed-beds. Mathematical formulations are presented followed by the presentation of dimensionless groups relevant to the considered models. Finally simulation results of single-blow operations are presented for illustrational purposes.

2. MATHEMATICAL FORMULATIONS

2.1 Common Definitions

Consider a porous medium composed of a solid desiccant material. The total volume occupied by this material $\mathcal{V}$ can subdivided into:

$$\mathcal{V} = \mathcal{V}_s + \mathcal{V}_\delta + \mathcal{V}_i + \mathcal{V}_\pi = \mathcal{V}_p + \mathcal{V}_i, \tag{1}$$

where $\mathcal{V}_s$ is the actual pore-free solid volume and $\mathcal{V}_\delta$ corresponds to the dead-end closed pore (unusable) volume. The volume $\mathcal{V}_i$ corresponds to voids between desiccant particles, which applies to fixed-bed operations. For desiccant-coated channels, the channel walls are modeled as a monolithic desiccant such that $\mathcal{V}_i = 0$. Finally the volume $\mathcal{V}_\pi$ corresponds to the interconnected pores, within desiccant particles (fixed-beds) or in the porous walls of desiccant wheel channels.

Considering that the voids are evenly distributed within the porous medium, the total porosity (usable), the porosity of the bed (for fixed-beds) and the particle (or a the channel wall itself) porosity are defined as:

$$\epsilon = \frac{\mathcal{V}_i + \mathcal{V}_\pi}{\mathcal{V}}, \qquad \epsilon_b = \frac{\mathcal{V}_i}{\mathcal{V}}, \qquad \varepsilon_p = \frac{\mathcal{V}_\pi}{\mathcal{V}_p}. \tag{2}$$

Naturally, for desiccant-coated channels $\varepsilon_b = 0$ and $\varepsilon_p = \epsilon$. The total porosity is related to bed and particle porosity as:

$$(1 - \epsilon) = (1 - \varepsilon_b)(1 - \varepsilon_p). \tag{3}$$

Finally, the structural volume of the particle is defined as the volumetric fraction occupied by empty solids and closed pores, so it can be written as:

$$\mathcal{V}_s + \mathcal{V}_\delta = (1 - \varepsilon_p)\mathcal{V}_p. \tag{4}$$

Assuming that the solid mass is uniformly distributed within the medium, the specific mass (also referred to as the true specific mass), which includes the solid volumes and the closed pores, is defined as:

$$\rho_s = \frac{\delta m_s}{\delta \mathcal{V}_s + \delta \mathcal{V}_\delta}. \tag{5}$$

In addition, the density of the dry porous bed and particles may be written as:

$$\rho_b = \frac{\delta m_s}{\delta \mathcal{V}}, \qquad \rho_p = \frac{\delta m_s}{\delta \mathcal{V}_p}. \tag{6}$$

The specific mass of water vapor, which can take on different values within pores and void space between particles, is written in different forms for each void space:

$$\rho_{v,\pi} = \frac{\delta m_{v,\pi}}{\delta \mathcal{V}_\pi} = \frac{\delta m_{v,\pi}}{\varepsilon_p \delta \mathcal{V}_p} = \frac{\delta m_{v,\pi}}{\varepsilon_p (1 - \varepsilon_b)\delta \mathcal{V}}, \qquad \rho_{v,i} = \frac{\delta m_{v,i}}{\delta \mathcal{V}_i} = \frac{\delta m_{v,i}}{\varepsilon_b \delta \mathcal{V}} \tag{7}$$

The density of dry air is assumed to be uniform within particle voids and inter-particle void space, and is expressed in terms of void spaces, excluding closed pores:

$$\rho_a = \frac{\delta m_a}{\delta \mathcal{V}_i + \delta \mathcal{V}_\pi} = \frac{\delta m_{g,i}}{\delta \mathcal{V}_i} = \frac{\delta m_{g,\pi}}{\delta \mathcal{V}_\pi} \tag{8}$$

The concentration of the adsorbed phase is defined in terms of the total volume:

$$\rho_l = \frac{\delta m_l}{\delta \mathcal{V}}. \tag{9}$$

In this type of analysis (provided that the concentration of water in the natural gas is considered diluted) it is convenient to express the concentrations on a dry basis as follows:

$$Y = \frac{\delta m_{v,i}}{\delta m_{g,i}} = \frac{\rho_{v,i}}{\rho_a}, \qquad Y_p = \frac{\delta m_{v,\pi}}{\delta m_{g,\pi}} = \frac{\rho_{v,\pi}}{\rho_a}, \qquad W = \frac{\delta m_l}{\delta m_s} = \frac{\rho_l}{\rho_b} = \frac{\rho_l}{\rho_s(1-\epsilon)} = \frac{\rho_l}{\rho_s\,(1-\epsilon_p)\,(1-\epsilon_b)}. \tag{10}$$

2.2 Fixed-bed model

A formulation for dehumidification of natural gas was developed in (Benther and Sphaier, 2015). This formulation can be readily adapted for moist air, leading to the following governing equations:

$$(1-\varepsilon_b)\left[\frac{\rho_p}{\rho_a}\frac{\partial W}{\partial t} + \varepsilon_p\frac{\partial Y_p}{\partial t}\right] = h_m\,(Y-Y_p)\,\mathcal{S}, \tag{11a}$$

$$\varepsilon_b\frac{\partial Y}{\partial t} + v_b\frac{\partial Y}{\partial x} = -h_m\,(Y-Y_p)\,\mathcal{S}, \tag{11b}$$

$$(1-\varepsilon_b)\frac{\rho_e\,\tilde{c}_e}{\rho_a}\frac{\partial T_p}{\partial t} = \left((1-\varphi)\,i^i_{sor}\,h_m\,(Y-Y_p) + \frac{h_h}{\rho_a}\,(T-T_p)\right)\mathcal{S} + \frac{\rho_b}{\rho_a}\,i^p_{sor}\frac{\partial W}{\partial t}, \tag{11c}$$

$$\tilde{c}\left(\varepsilon_b\frac{\partial T}{\partial t} + v_b\frac{\partial T}{\partial x}\right) = \left(\varphi\,i^i_{sor}\,h_m\,(Y-Y_p) - \frac{h_h}{\rho_a}\,(T-T_p)\right)\mathcal{S}, \tag{11d}$$

which comprise, respectively, mass conservation balances for water vapor in desiccant particles ($\mathcal{V}_p$) and in the intra-particle space ($\mathcal{V}_i$), and energy conservation balances for the same volumes. The specific area $\mathcal{S}$ represents the surface area of particles $\mathcal{A}_s$ divided by the bulk volume $\mathcal{V}$. The effective heat capacities $\rho_a\,\tilde{c}$ and $\rho_e\,\tilde{c}_e$ are defined as:

$$\rho_a\,\tilde{c} = \rho_a\,(c_{p,a} + c_{p,v}\,Y)\,, \tag{12a}$$

$$\rho_e\,\tilde{c}_e = \rho_p\,(c_s + c_l\,W) + \varepsilon_p\,\rho_a\,(c_{p,a} + c_{p,v}\,Y_p). \tag{12b}$$

and $1-\varphi$ is the fraction of i^i_{sor} that contributes directly to heating (or cooling) the gas stream; conversely, φ is the fraction of i^i_{sor} that contributes directly to heating (or cooling) the adsorbent particles, which are defined in terms of the film transfer enthalpy, $i_{v,f}$:

$$1-\varphi = \frac{i_{v,f}-i_{v,\pi}}{i_{v,i}-i_{v,\pi}}, \qquad \varphi = \frac{i_{v,i}-i_{v,f}}{i_{v,i}-i_{v,\pi}}. \tag{13}$$

Also, the bed velocity v_b (or bulk velocity) can be related to the inter-particle velocity v using the the bed porosity

$$v_b = v\,\varepsilon_b, \tag{14}$$

and the sensible heat of sorption i^i_{sor} can be written in terms of the temperature change $T-T_p$:

$$i^i_{sor} = c_{p,v}\,(T-T_p). \tag{15}$$

2.3 Channels with desiccant-coated walls

A one-dimensional formulation that considerers heat and mass transfer within a desiccant wheel's mini-channels and solid walls, as described in (Sphaier and Worek, 2006; Sphaier, 2014), is recalled. Additional simplifications such as a single-blow operation, no supporting structure, and negligible axial diffusion is considered, leading to the following governing equations:

$$\mathcal{A}_f\left[\frac{\rho_p}{\rho_a}\frac{\partial W}{\partial t} + \varepsilon_p\frac{\partial Y_p}{\partial t}\right] = h_m\,(Y-Y_p)\,\mathcal{P}_s, \tag{16a}$$

$$\mathcal{A}_p\left(\frac{\partial Y}{\partial t} + v\frac{\partial Y}{\partial x}\right) = -h_m\,(Y-Y_p)\,\mathcal{P}_s, \tag{16b}$$

$$\mathcal{A}_f\,\frac{\rho_e\,\tilde{c}_e}{\rho_a}\frac{\partial T_p}{\partial t} = \left((1-\varphi)\,i^i_{sor}\,h_m\,(Y-Y_p) + \frac{h_h}{\rho_a}\,(T-T_p)\right)\mathcal{P}_s + \mathcal{A}_f\,\frac{\rho_p}{\rho_a}\,i^p_{sor}\frac{\partial W}{\partial t}, \tag{16c}$$

$$\mathcal{A}_p\,\tilde{c}\left(\frac{\partial T}{\partial t} + v\frac{\partial T}{\partial x}\right) = \left(\varphi\,i^i_{sor}\,h_m\,(Y-Y_p) - \frac{h_h}{\rho_a}\,(T-T_p)\right)\mathcal{P}_s, \tag{16d}$$

which comprise, respectively, mass conservation balances for water vapor in the porous channel wall ($\mathcal{V}_p$ with $\mathcal{V}_i=0$) and in the airstream that flows within channels, as well as energy conservation balances for the same spaces. The geometric quantities $\mathcal{P}_s$, $\mathcal{A}_p$ a nd $\mathcal{A}_f$ respectively correspond to the wetted perimeter of channels (surface area between airstream and desiccant material divided by channel length), the flow area, and the area of the desiccant material (volume per channel length) .

Treating the entire regenerator matrix as a macro porous medium, an equivalent bed-porosity may be defined, based on the volume (or area) relations, followed by a specific surface area:

$$\varepsilon_b = \frac{\mathcal{A}_p\,L}{(\mathcal{A}_p+\mathcal{A}_f)\,L}, \qquad 1-\varepsilon_b = \frac{\mathcal{A}_f\,L}{(\mathcal{A}_p+\mathcal{A}_f)\,L}, \qquad \mathcal{S} = \frac{\mathcal{P}_s\,L}{(\mathcal{A}_p+\mathcal{A}_f)\,L}. \tag{17}$$

2.4 Unified formulation

Using equations (17) and (14) one can readily perceive that the two sets of governing equations lead to the exact same formulation. With these consideration one can note that adding equations adding equations (11a) and (11b) (or (16a) and (16b)), and also equations (11c) and (11d) (or (16c) and (16d)) respectively gives:

$$(1-\varepsilon_b)\left[\frac{\rho_p}{\rho_a}\frac{\partial W}{\partial t} + \varepsilon_p\frac{\partial Y_p}{\partial t}\right] + \varepsilon_b\left(\frac{\partial Y}{\partial t} + v\frac{\partial Y}{\partial x}\right) = 0, \tag{18a}$$

$$(1-\varepsilon_b)\frac{\rho_e\,\tilde{c}_e}{\rho_a}\frac{\partial T_p}{\partial t} + \tilde{c}\,\varepsilon_b\left(\frac{\partial T}{\partial t} + v\frac{\partial T}{\partial x}\right) = i^i_{sor}\,h_m\,(Y-Y_p)\,\mathcal{S} + \frac{\rho_b}{\rho_a}\,i^p_{sor}\frac{\partial W}{\partial t}, \tag{18b}$$

which clearly shows that the total heating (or cooling) effect can be subdivided into a sensible-only part (containing i^i_{sor}) and a latent part (containing i^p_{sor}).

3. NORMALIZATION

The normalization of the governing equations is carried out by introducing the following non-dimensional variables:

$$x^* = \frac{x}{L}, \qquad t^* = \frac{t}{\tau}, \qquad T^* = \frac{T-T_{\min}}{\Delta T}, \qquad Y^* = \frac{Y}{Y_{\max}}, \tag{19}$$

$$T^*_p = \frac{T_p-T_{\min}}{\Delta T}, \qquad Y^*_p = \frac{Y_p}{Y_{\max}}, \qquad Y^*_p = \frac{Y_p}{Y_{\max}}, \qquad W^* = \frac{W}{W_{\max}}, \tag{20}$$

where $\Delta T = T_{\max} - T_{\min}$. The substitution of these variables into the governing equations (eqs. (11) or (16)) leads to the following equations:

$$\Omega\frac{\partial W^*}{\partial t^*} + \frac{\partial Y^*_p}{\partial t^*} = \frac{\mathrm{NTU}_m}{\mathrm{V}^*_r}(Y^*-Y^*_p), \tag{21a}$$

$$\left(\tau_{dw}\frac{\partial Y^*}{\partial t^*} + \frac{\partial Y^*}{\partial x^*}\right) = -\mathrm{NTU}_m\,(Y^*-Y^*_p), \tag{21b}$$

$$\chi_f\frac{\partial T^*_p}{\partial t^*} = \frac{\mathrm{NTU}_h}{\mathrm{C}^*_r}(T^*-T^*_p) + \frac{\mathrm{NTU}_m}{\mathrm{V}^*_r}\frac{c^*_p}{c^*_s}(1-\varphi)\,(Y^*-Y^*_p)\,\left(T^*-T^*_p\right) + i^*_{sor}\frac{\partial W^*}{\partial t^*}, \tag{21c}$$

$$\chi\left(\tau_{dw}\frac{\partial T^*}{\partial t^*} + \frac{\partial T^*}{\partial x^*}\right) = \mathrm{NTU}_m\,\varphi\,c^*_p\,(Y^*-Y^*_p)\,(T^*-T^*_p) - \mathrm{NTU}_h\,(T^*-T^*_p), \tag{21d}$$

Where the involved dimensionless parameters are defined below. The dimensionless dwell time and numbers of transfer units are given by:

$$\tau_{dw} = \frac{L}{v\,\tau}, \qquad \mathrm{NTU}_m = \frac{L}{v}\frac{\mathcal{P}_s}{\mathcal{A}_p}h_m = \frac{L}{v}\frac{\mathcal{S}}{\varepsilon_b}h_m, \qquad \mathrm{NTU}_h = \frac{L}{v}\frac{\mathcal{P}_s}{\mathcal{A}_p}\frac{h_h}{\rho_a\,c_{p,a}} = \frac{L}{v}\frac{\mathcal{S}}{\varepsilon_b}\frac{h_h}{\rho_a\,c_{p,a}}, \tag{22a}$$

The dimensionless maximum water uptake and the dimensionless heat of sorption are given by:

$$\Omega = \frac{1-\varepsilon_p}{\varepsilon_p}\left(\frac{\rho_s}{\rho_a}\frac{W_{\max}}{Y_{\max}}\right) = \frac{1}{\varepsilon_p}\left(\frac{\rho_p}{\rho_a}\frac{W_{\max}}{Y_{\max}}\right), \qquad i^*_{sor} = \frac{i^p_{sor}\,W_{\max}}{c_s\,\Delta T}. \tag{22b}$$

The dimensionless volumetric and heat capacity ratios are given by:

$$\mathrm{V}^*_r = \frac{L}{v\,\tau}\frac{\varepsilon_p\,\mathcal{A}_f}{\mathcal{A}_p} = \frac{L}{v\,\tau}\frac{\varepsilon_p\,(1-\varepsilon_b)}{\varepsilon_b}, \qquad \mathrm{C}^*_r = \frac{L}{v\,\tau}\frac{(1-\varepsilon_p)\,\rho_s\,c_s\,\mathcal{A}_f}{\rho_a\,c_{p,a}\,\mathcal{A}_p} = \frac{L}{v\,\tau}\frac{(1-\varepsilon_p)\,\rho_s\,c_s\,(1-\varepsilon_b)}{\rho_a\,c_{p,a}\,\varepsilon_b}, \tag{22c}$$

Additional heat capacity ratios are also defined:

$$c^*_p = \frac{c_{p,v}\,Y_{\max}}{c_{p,a}}, \qquad c^*_l = \frac{c_l\,W_{\max}}{c_s}, \qquad c^*_s = \frac{(1-\varepsilon_p)\,\rho_s\,c_s}{\varepsilon_p\,\rho_a\,c_{p,a}}, \tag{22d}$$

and additional dimensionless coefficients that take into account variations in the thermophysical properties mainly due to variations in water content are defined as well:

$$\chi = \frac{\rho_a\,\tilde{c}}{\rho_a\,c_{p,a}} = 1 + c^*_p\,Y^*, \qquad \chi_f = \frac{\rho_f\,c_f}{(1-\epsilon)\rho_s\,c_s} = 1 + c^*_l\,W^* + \frac{\mathrm{V}^*_r}{\mathrm{C}^*_r}\,(1+Y^*_p\,c^*_p)\,(1-\varepsilon_b)\,\varepsilon_p, \tag{23}$$

where the specific heat of the adsorbed water is calculated through:

$$c_l = c_{ls} + \frac{1}{W}\left(\frac{\partial\Delta i_w}{\partial T_p}\right)_W, \tag{24}$$

where c_{ls} is the specific heat of saturated liquid water and Δi_w is the integral heat of wetting.

4. NUMERICAL SOLUTION

The normalized formulation is solved numerically using a simple first-order uniform-grid upwind discretization scheme using the finite volumes method. All equations are integrated within a 1D control volume of length $\Delta x^* = x^*_{i+1/2} - x^*_{i-1/2}$ using the operator $\int_{x^*_{i-1/2}}^{x^*_{i+1/2}} \bullet \, \mathrm{d}x^*$ and all integrals are approximated using a second order approximation rule:

$$\int_{x^*_{i-1/2}}^{x^*_{i+1/2}} f(x^*, t^*)\, \mathrm{d}x^* \;\approx\; f(x^*_i, t^*)\, \Delta x^*. \tag{25}$$

Where $i = 1, 2, \ldots, i_{\max}$, corresponds do the computational grid points, located at positions $x^*_i = \Delta x^* \, (i - 1/2)$, with $\Delta x^* = 1/i_{\max}$. Next, all spatial derivatives are approximated as

$$\int_{x^*_{i-1/2}}^{x^*_{i+1/2}} \frac{\partial f}{\partial x^*}\, \mathrm{d}x^* \;=\; \frac{f_{i+1/2} - f_{i-1/2}}{\Delta x^*} \;\approx\; \frac{f_i - f_{i-1}}{\Delta x^*}. \tag{26}$$

These results in the following discretized system of equations:

$$\Omega \, \frac{\mathrm{d}(W^*)_i}{\mathrm{d}t^*} \;+\; \frac{\mathrm{d}(Y^*_p)_i}{\mathrm{d}t^*} \;=\; \frac{\mathrm{NTU}_m}{\mathrm{V}^*_r} (Y^* - Y^*_p)_i, \tag{27a}$$

$$\tau_{dw} \, \frac{\mathrm{d}(Y^*)_i}{\mathrm{d}t^*} \;+\; \frac{(Y^*)_i - (Y^*)_{i-1}}{\Delta x^*} \;=\; -\mathrm{NTU}_m \, (Y^* - Y^*_p)_i, \tag{27b}$$

$$(\chi_f)_i \, \frac{\mathrm{d}(T^*_p)_i}{\mathrm{d}t^*} \;=\; \frac{\mathrm{NTU}_h}{\mathrm{C}^*_r} (T^* - T^*_p)_i \;+\; \frac{\mathrm{NTU}_m}{\mathrm{V}^*_r} \, \frac{c^*_p}{c^*_s} \, (1 - \varphi) \, (Y^* - Y^*_p)_i \, (T^* - T^*_p)_i \;+\; i^*_{sor} \, \frac{\mathrm{d}(W^*)_i}{\mathrm{d}t^*}, \tag{27c}$$

$$(\chi)_i \left(\tau_{dw} \frac{\mathrm{d}(T^*)_i}{\mathrm{d}t^*} + \frac{(T^*)_i - (T^*)_{i-1}}{\Delta x^*} \right) = \mathrm{NTU}_m \, \varphi \, c^*_p \, (Y^* - Y^*_p)_i \, (T^* - T^*_p)_i \;-\; \mathrm{NTU}_h \, (T^* - T^*_p)_i, \tag{27d}$$

which are valid for $i = 2, \ldots, i_{\max}$. For the inlet cell ($i = 1$), equations (27a) and (27c) are still valid, but equations (27b) and (27d) need to be modified to:

$$\tau_{dw} \, \frac{\mathrm{d}(Y^*)_i}{\mathrm{d}t^*} \;+\; \frac{(Y^*)_i - (Y^*)_{in}}{\Delta x^*/2} \;=\; -\mathrm{NTU}_m \, (Y^* - Y^*_p)_i, \tag{28a}$$

$$(\chi)_i \left(\tau_{dw} \frac{\mathrm{d}(T^*)_i}{\mathrm{d}t^*} + \frac{(T^*)_i - (T^*)_{in}}{\Delta x^*/2} \right) = \mathrm{NTU}_m \, \varphi \, c^*_p \, (Y^* - Y^*_p)_i \, (T^* - T^*_p)_i \;-\; \mathrm{NTU}_h \, (T^* - T^*_p)_i, \tag{28b}$$

where the subscript in indicates the inlet conditions $Y^*(0, t^*) = Y^*_{in}$ and $T^*(0, t^*) = T^*_{in}$. This system of ODEs is finally solved using the mathematica function **NDSolve**, starting from an initial condition given by:

$$Y^*(x^*, 0) \;=\; Y^*_0, \qquad T^*(x^*, 0) \;=\; T^*_0. \tag{29}$$

Finally the relation between W^*, Y^*_p and T^*_p is calculated using a simple linear isotherm

$$W^* \;=\; \phi(Y^*_p, T^*_p), \tag{30}$$

for which ϕ is represents the relative humidity, given in terms of the water vapor pressure p_v

$$\phi \;=\; \frac{p_v}{p_{sat}(T)}, \quad \text{with} \quad p_v \;=\; \frac{Y_p \, p}{r_M + Y_p}, \tag{31}$$

where $r_M = 18.02/28.97$ is the ratio of the molecular masses of water and air, p is the total pressure of moist air (atmospheric for the current application), and p_{sat} is the vapor saturation pressure (gas-liquid interface), which is calculated by the formulas provided by Hyland and Wexler (1983).

5. RESULTS AND DISCUSSION

This section presents illustrative results of the numerical solution of the considered problem. Table 1 presents the numerical data used in the simulations. The dimensional data were obtained from previous works (Sphaier and Worek, 2004, 2009), while the dimensionless data were calculated from the dimensional data, with the exception of the number of transfer units, for which typical values were used for part of the results ($\mathrm{NTU}_m = \mathrm{NTU}_h = 10$), and then varied in the last simulations. It is important to point out that the considered situations corresponds to an initially hot and dry desicant material, which is then subjected to a moist airstream at a typical condition for cities in Brazilian ($T_{in} = 30C$, $\phi = 50\%$).

Table 1. Data used in simulations.

dimensional data							
$T_{\max}$	120ºC	$T_{\min}$	30ºC	T_{in}	30ºC	T_0	120ºC
$\phi_{\max}$	1	ϕ_{in}	0.5	ϕ_0	0.5	ϵ_p	0.3
L	0.4 m	v	5 m/s	τ	60 s	ϵ_b	0.5
$c_{p,a}$	1.0 $\frac{kJ}{kg.K}$	$c_{p,v}$	1.8 $\frac{kJ}{kg.K}$	c_s	0.7 $\frac{kJ}{kg.K}$	c_l	4.18 $\frac{kJ}{kg.K}$
ρ_a	1 $\frac{kg}{m^3}$	ρ_s	1200 $\frac{kg}{m^3}$	$Y_{\max}$	0.027206	i_{sor}	3001.2 $\frac{kJ}{kg}$
dimensionless data							
c_s^*	1960	c_p^*	0.0489707	c_l^*	2.38857		
Ω	41167.4	i_{sor}^*	19.0552	τ_{dw}	0.00133333	Y_{in}^*	0.4893
V_r^*	0.0004	C_r^*	0.336	φ	0.5	T_{in}^*	0

Table 2. Convergence analysis: outlet temperature and humidity ratio.

$i_{\max}$	$Y^*(0.001)$	$T^*(0.001)$	$Y^*(0.01)$	$T^*(0.01)$	$Y^*(0.1)$	$T^*(0.1)$	$Y^*(1)$	$T^*(1)$
10	0.4266	0.9666	0.0219	0.2445	0.1298	0.1419	0.4790	0.0040
20	0.4391	0.9751	0.0187	0.2354	0.1197	0.1459	0.4810	0.0032
40	0.4465	0.9797	0.0171	0.2300	0.1138	0.1482	0.4822	0.0028
80	0.4505	0.9820	0.0164	0.2270	0.1105	0.1495	0.4828	0.0025
160	0.4526	0.9832	0.0160	0.2255	0.1088	0.1502	0.4831	0.0024
320	0.4537	0.9838	0.0158	0.2247	0.1079	0.1505	0.4832	0.0024
640	0.4542	0.9841	0.0157	0.2243	0.1074	0.1507	0.4833	0.0023

The first results are dedicated to demonstrating the convergence behavior of the numerical solution, as shown in table 2. Outlet values for the dimensionless temperature and concentration of the airstream are presented for different values of non-dimensional time ($t^* = 0.001, 0.01, 0.1$ and 1). As can be seen, with the exception of outlet temperature values at $t^* = 1$ a relative error of less than 1% is obtained for all cases even for grid-sizes coarser than 640 divisions, which is suitable for all graphical analysis that are subsequently presented. For the temperature values at $t^* = 1$, these are near-zero values, which are obtained when thermal equilibrium is almost reached. As this values will show as zero in all plots, the employed grid and numerical solution are considered suitable for the analysis herein presented.

The next results illustrate the temperature, water concentrations, and relative humidity distributions within the porous matrix in the airstream, as portrayed in figure 1. As one can observe the system initially goes through a quick cooling due to colder inlet airstream. After this water starts to be adsorbed which is seen by the rise of W^* values while Y_p^* values diminish – and consequently Y^* are also reduced, but with a delay due to the mass transfer resistance between the desiccant particles and free airstream. Adsorption continues to occur – which is seen by ongoing rising value of W^*, while Y^* values are clearly larger than Y_p^* (up until about $t^* = 0.1$). After this time the desiccant material starts to become saturated (approaching $W^* = \phi_{in} = 0.5$), and the system tends to thermodynamic equilibrium, for which all temperature and humidity values become equal to the inlet condition ($T_{in}^* = 0$ and $\phi_{in} = 0.5$).

The final results illustrate the effect of varying the number of transfer units for heat and mass transfer, while maintaining all other parameter values, as displayed in figure 2. The outlet values for the the dimensionless temperature, dimensionless humidity ratio and relative humidity varying over the dimensionless time range are shown for different values of the number of transfer units, considering $\mathrm{NTU}_h = \mathrm{NTU}_m$. As one can observe from these results, different regimes can be noted from these solutions, which become more evident as the number of transfers units are increase. Looking at the case with $\mathrm{NTU}_m = \mathrm{NTU}_h = 100$, these are evidently separated. An initial regime corresponding to the sensible cooling of the warm desiccant occurs up until $t^* = 0.005$. Form this value to about $t^* = 0.1$ a dehumidification regime takes place, for which the outlet water concentration is nearly zero (while the inlet concentration is that corresponding to $\phi = 0.5$). For this last regime the outlet temperature is somewhat higher than the inlet temperature and remains at a constant plateau due to the heating effect associated with the sorption phenomena. Finally, a last regime is seen, corresponding to the further cooling of the material after it becomes saturated (occurring between $t^* = 0.1$ and $t^* = 0.5$). As the material gradually looses its adsorption capacity, the outlet humidity values rise to the inlet condition. For $t^* > 0.5$ thermodynamic equilibrium has been roughly reached, and all outlet values tend to match the inlet conditions. As the number of transfer units are reduced the regimes can still be noted, however, less clearly, especially for very low NTU values. Lower NTU values also seem to imply in longer periods for each of these regimes, and consequently a longer time for reaching thermodynamic equilibrium.

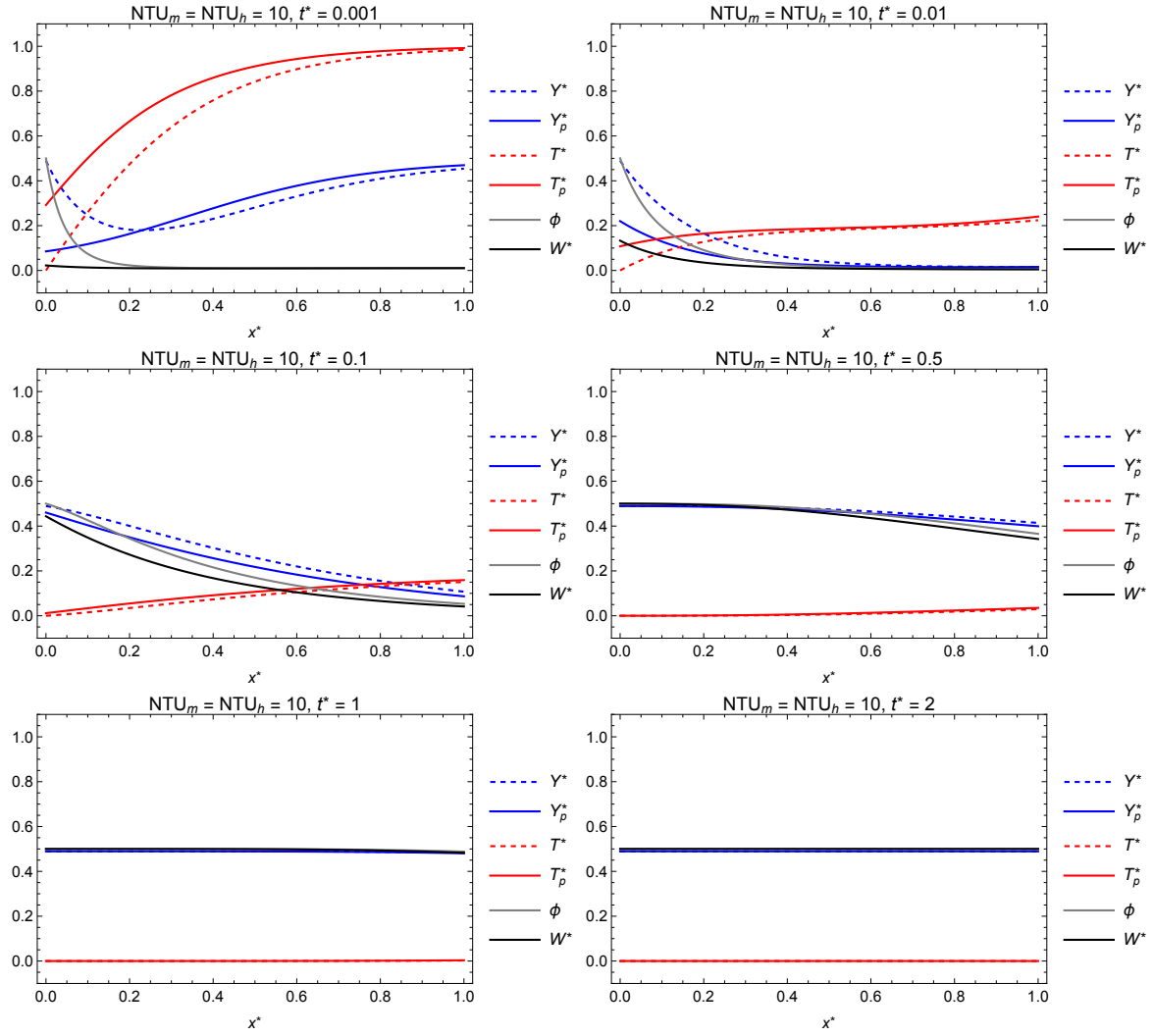

Figure 1. Temperature and humidity distribution at different instants.

6. SUMMARY AND CONCLUSIONS

This paper presented simple one-dimensional formulations for two type of desiccant dehumidification systems, namely fixed-bed systems, and desiccant coated channels (as found in desiccant wheels). Then, a unified formulation, valid for both configurations, was proposed. This formulation was normalized using typical dimensionless groups for this type of problem. The systems consists of four coupled non-linear PDEs for heat and mass transfer within the desiccant material and within the void spaces between desiccant particles (or in a free stream in a channel). A simple finite-volume based solution using a first-order upwind discretization scheme is employed, leading to a discretized ODE system, which is then time-integrated using the Mathematica function NDSolve. A convergence analysis of the solution is then presented, verifying that the solution indeed converges and determining which grid size is adequate for the posterior analysis. Ultimately, illustrative results are presented to show the evolution of the temperature and water concentration distributions, and the effects of varying the number of transfer units. The results lead to interesting conclusions such as the clear distinction of three different regimes, those of which become more evident for higher NTU values.

7. ACKNOWLEDGEMENTS

The authors would like to acknowledge the financial support provided by the National Agency of Petroleum ANP, as well as the support provided by Federal University of Fluminense (UFF) Brazil.

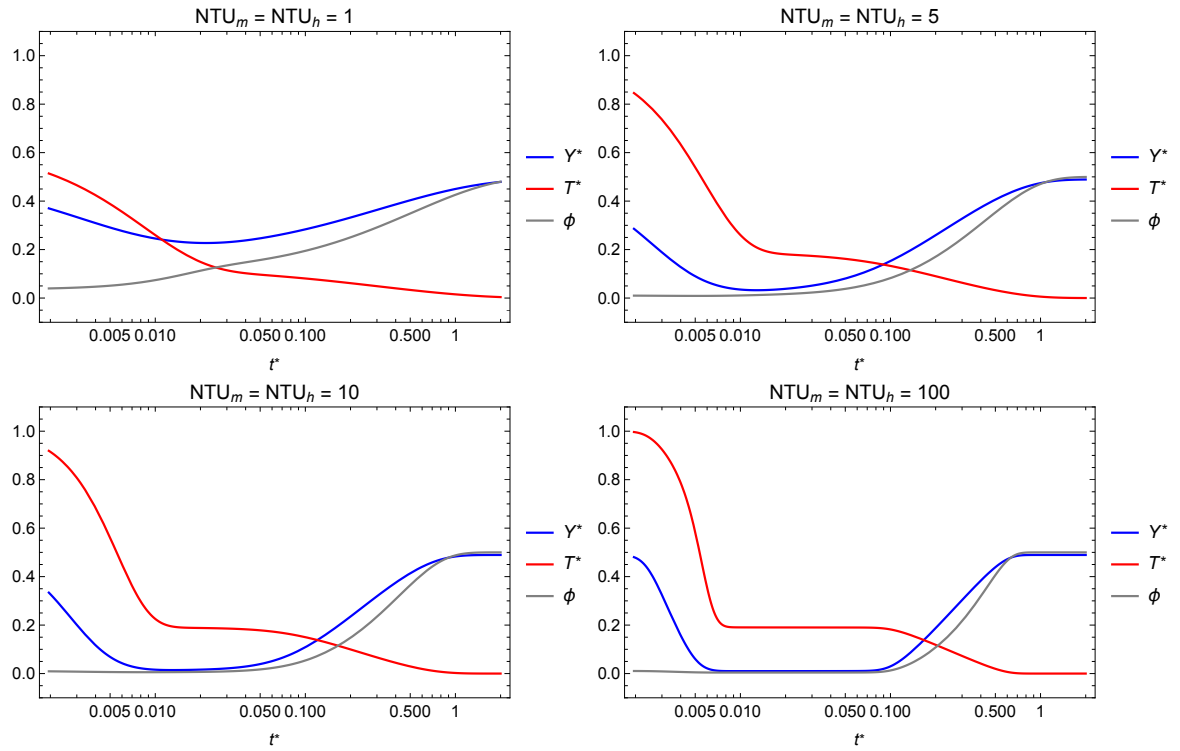

Figure 2. Outlet temperature and humidity for different number of heat and mass transfer units.

8. REFERENCES

Beery, K.E. and Ladisch, M.R., 2001. "Chemistry and properties of starch based desiccants". *Enzyme and Microbial Technology*, Vol. 28, No. 7-8, pp. 573–581.

Benther, J.D. and Sphaier, L.A., 2015. "One-dimensional formulation for heat and mass transfer in solid desiccant dehydration of natural gas". *Heat Transfer Engineering*, Vol. 36, No. 11, pp. 952–962.

Cheng, D., Peters, E.F. and Kuipers, J.H., 2016. "Numerical modelling of flow and coupled mass and heat transfer in an adsorption process". *Chemical Engineering Science*, Vol. 152, pp. 413–425.

Cheng, D., Peters, E.F. and Kuipers, J.H., 2017. "Performance study of heat and mass transfer in an adsorption process by numerical simulation". *Chemical Engineering Science*, Vol. 160, pp. 335–345.

Chung, J.D., Lee, D.Y. and Yoon, S.M., 2009. "Optimization of desiccant wheel speed and area ratio of regeneration to dehumidification as a function of regeneration temperature". *Solar Energy*, Vol. 83, No. 5, pp. 625–635.

Dai, Y., Wang, R. and Zhang, H., 2001. "Parameter analysis to improve rotary desiccant dehumidification using a mathematical model". *International journal of thermal sciences*, Vol. 40, No. 4, pp. 400–408.

DAOU, K., WANG, R. and XIA, Z., 2006. "Desiccant cooling air conditioning: a review". *Renewable and Sustainable Energy Reviews*, Vol. 10, No. 2, pp. 55–77.

Ge, T., Ziegler, F. and Wang, R., 2010. "A mathematical model for predicting the performance of a compound desiccant wheel (a model of compound desiccant wheel)". *Applied Thermal Engineering*, Vol. 30, No. 8-9, pp. 1005–1015.

Hougen, O.A. and Marshall, W.R.J., 1947. "Adsorption from a fluid stream flowing through a stationary granular bed." *Chem Eng Prog 43(4):197–208.*

Hyland, R.W. and Wexler, A., 1983. "Formulations for the thermodynamic properties of the saturated phases of H2O from 173.15 K to 473.15 K". *ASHRAE transactions*, Vol. 89, pp. 500–519.

Jani, D., Mishra, M. and Sahoo, P.K., 2016. "Solid desiccant air conditioning–a state of the art review". *Renewable and sustainable energy reviews*, Vol. 60, pp. 1451–1469.

Jedlikowski, A., Kanaś, P. and Anisimov, S., 2020. "Heat and mass transfer inside the rotary heat exchanger operating under high speed rotor conditions". *International Journal of Heat and Mass Transfer*, Vol. 152, p. 119558.

Li, Z., Liu, X.H., Lun, Z. and Jiang, Y., 2010. "Analysis on the ideal energy efficiency of dehumidification process from buildings". *Energy and Buildings*, Vol. 42, No. 11, pp. 2014–2020.

Ruivo, C., Costa, J. and Figueiredo, A., 2007. "On the behaviour of hygroscopic wheels: Part i – channel modelling". *International Journal of Heat and Mass Transfer*, Vol. 50, No. 23-24, pp. 4812–4822.

Santos, S. and Sphaier, L., 2020. "Transient formulation for evaluating convective coefficients in regenerative exchangers with hygroscopic channels". *International Communications in Heat and Mass Transfer*, Vol. 116, p. 104691.

Shang, W. and Besant, R., 2009. "Effectiveness of desiccant coated regenerative wheels from transient response charac-

teristics and flow channel properties—part i: Development of effectiveness equations from transient response characteristics". *HVAC&R Research*, Vol. 15, No. 2, pp. 329–345.

Sphaier, L.A., 2014. "Mathematical modeling of heat and mass transfer in regenerators with desiccant materials". In *Desiccant-Assisted Cooling*, Springer London, pp. 47–83.

Sphaier, L.A. and Worek, W.M., 2006. "Comparisons between 2-d and 1-d formulations of heat and mass transfer in rotary regenerators". *Numerical Heat Transfer, Part B: Fundamentals*, Vol. 49, No. 3, pp. 223–237.

Sphaier, L.A. and Worek, W.M., 2009. "Parametric analysis of heat and mass transfer regenerators using a generalized effectiveness-NTU method". *International Journal of Heat and Mass Transfer*, Vol. 52, No. 9–10, pp. 2265–2272.

Sphaier, L. and Worek, W., 2004. "Analysis of heat and mass transfer in porous sorbents used in rotary regenerators". *International Journal of Heat and Mass Transfer*, Vol. 47, No. 14, pp. 3415–3430.

Wu, X., Ge, T., Dai, Y. and Wang, R., 2018. "Review on substrate of solid desiccant dehumidification system". *Renewable and Sustainable Energy Reviews*, Vol. 82, pp. 3236–3249.

Zhao, Y., Dai, Y., Ge, T., Sun, X. and Wang, R., 2015. "On heat and moisture transfer characteristics of a desiccant dehumidification unit using fin tube heat exchanger with silica gel coating". *Applied Thermal Engineering*, Vol. 91, pp. 308–317.

Zhehuadu and Lin, X., 2020. "Study on mathematical model of desiccant wheel". *IOP Conference Series: Earth and Environmental Science*, Vol. 512, No. 1, p. 012144.

9. RESPONSIBILITY NOTICE

The author(s) is (are) solely responsible for the printed material included in this paper.